

Zitterbewegung and bulk-edge Landau-Zener tunneling in topological insulators

Gerson J. Ferreira,¹ Renan P. Maciel,¹ Poliana H. Penteado,^{2,3} and J. Carlos Egues³

¹*Instituto de Física, Universidade Federal de Uberlândia, Uberlândia, Minas Gerais 38400-902, Brazil*

²*International Institute of Physics, Universidade Federal do Rio Grande do Norte, 59078-970 Natal-RN, Brazil*

³*Instituto de Física de São Carlos, Universidade de São Paulo, São Carlos, São Paulo 13560-970, Brazil*

 (Received 19 July 2018; published 15 October 2018)

We investigate the ballistic zitterbewegung dynamics and the Landau-Zener tunneling between edge and bulk states of wave packets in two-dimensional topological insulators. In bulk, we use the Ehrenfest theorem to show that an external in-plane electric field not only drifts the packet longitudinally, but also induces a transverse finite side-jump for both trivial and topological regimes. For finite ribbons of width W , we show that the Landau-Zener tunneling between bulk and edge states vanishes for large W as their electric-field-induced coupling decays with $W^{-3/2}$. This is demonstrated by expanding the time-dependent Schrödinger equation in terms of Houston states. Hence we cannot picture the quantum spin Hall states as arising from the zitterbewegung bulk trajectories “leaking” into the edge states, as proposed in *Phys. Rev. B* **87**, 161115(R) (2013).

DOI: [10.1103/PhysRevB.98.165120](https://doi.org/10.1103/PhysRevB.98.165120)

I. INTRODUCTION

The dynamics of wave packets in multiband systems presents a variety of interesting physical phenomena, e.g., the early studies of the Landau-Zener tunneling (LZT) [1–5], the ballistic spin resonance in multichannel spin-orbit coupled quantum wires [6,7], and the dynamics of unusual spin textures in spin-orbit coupled two-dimensional electron gases [8–13]. Moreover, the trembling motion, or zitterbewegung, is a particularly interesting dynamics that arises due to the spin-orbit coupling in quantum wells [14–18] and topological insulators (TIs) [19–21].

The topological insulators [22–26] are characterized by band inversions that lead to symmetry-protected helical edge/surface states with Dirac-like dispersion within the bulk gap. Recently, it was proposed [19] that the semiclassical zitterbewegung trajectories of electrically driven carriers in two-dimensional (2D) TIs could provide an intuitive picture for the dynamical emergence of the edge states. On the other hand, it is well known that in GaAs quantum wells the zitterbewegung is accompanied by a finite ballistic side jump [16]. This process leads to spin polarization at the edges, constituting a ballistic spin Hall effect in narrow wires [27]. In the diffusive regime, the side-jump accumulated after successive Markovian scatterings was recently related to the Rashba-Edelstein effect [28].

The zitterbewegung is usually calculated in bulk, while the edge states exist only at the borders of finite-size samples. Therefore, it is interesting to investigate the effects of both the edge states and the quantum confinement on the ballistic dynamics of wave packets in TI ribbons in the presence of electric fields. More importantly, does the corresponding zitterbewegung trajectories indeed bear any connection with the helical edge states as proposed in Ref. [19]?

In this paper, we address this issue by investigating the ballistic dynamics of electrically driven wave packets in 2D TIs fully accounting for the LZT between bulk and edge

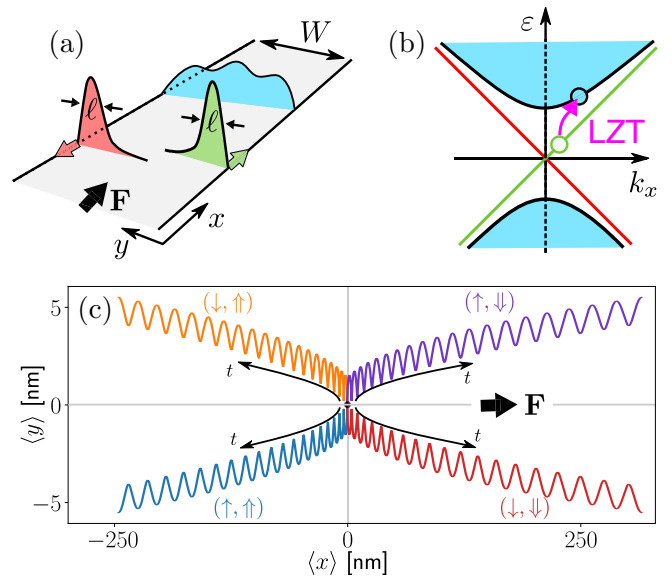


FIG. 1. (a) Illustration of a BHZ ribbon of width W with edge states, characterized by a penetration length ℓ , and a bulk state (blue). (b) Sketch of the BHZ band structure in the nontrivial regime with linear edge-state branches and bulk bands. The arrow indicates the Landau-Zener tunneling between an edge state and a bulk band promoted by the electric field \mathbf{F} . (c) zitterbewegung trajectories $[\langle x \rangle(t), \langle y \rangle(t)]$ in bulk for $0 < t < 5$ ps for different initial spin $s = \{\uparrow, \downarrow\}$ and pseudospin $\sigma_z = \{\uparrow, \downarrow\}$. For larger $t \gtrsim 50$ ps the motion along y saturates into a finite side-jump $|y(\infty)| \approx 18.75$ nm.

states. We model our system by the Bernevig-Hughes-Zhang (BHZ) Hamiltonian [22] in the presence of an external electric field \mathbf{F} . For a ribbon of width W , as illustrated in Figs. 1(a) and 1(b), we show that the LZT is characterized by the nondiagonal terms of the Berry connection matrix $\mathcal{A}_{k_x}^{n,n'}$. For $W \gg \ell$, where ℓ is the typical length of the edge states,

we find that the LZT vanishes with $W^{-3/2}$. In addition, we analyze the semiclassical zitterbewegung trajectories in bulk, which always show a finite ballistic side-jump [16] toward a direction that strongly depends on the initial conditions, Fig. 1(c).

For a finite ribbon, we solve the Schrödinger equation numerically and study the full dynamics of a wave packet. Consistently with $\mathcal{A}_{k_x}^{n,n'}$ vanishing for $W \gg \ell$, we show that a Gaussian wave packet bounces off the borders of the ribbon unaffected by the presence of the edge states. These results do not support the idea from Ref. [19] that the helical edge states emerge from the bulk zitterbewegung trajectories, which would provide a semi-classical picture of the quantum spin Hall effect (QSHE). Instead, the zitterbewegung and finite ballistic side-jump seen here are compatible with the GaAs Rashba-Edelstein effect from Ref. [28], which was already suggested [16] as a semiclassical picture of the spin Hall effect (SHE).

This paper is organized as follows. In Sec. II, we present the model Hamiltonian and the numerical parameters. In Sec. III, we discuss the Landau-Zener tunneling and its dependence on the system size. In Secs. IV and V, we present results for the zitterbewegung, using the Ehrenfest theorem and the full time evolution of a wave packet for large systems, respectively. We finally summarize our findings in Sec. VI.

II. MODEL SYSTEM

We consider the BHZ Hamiltonian [22]

$$H = C - D\mathbf{k}^2 + sAk_x\sigma_x + Ak_y\sigma_y + (M - Bk^2)\sigma_z, \quad (1)$$

where $s = \pm 1$ labels the spin-up (\uparrow) and -down (\downarrow) subspaces, σ are the Pauli matrices acting on the pseudospin subspace $\{E_1, H_1\} = \{\uparrow, \downarrow\}$ of the confined electron and hole states of the quantum well, and $\mathbf{k} = (k_x, k_y)$ are the in-plane momenta. Unless otherwise specified, we choose typical values for the parameters [23]: $C = 6.5$ meV, $A = 375$ meV nm, $B = -1120$ meV nm², $D = -730$ meV nm², and a negative Dirac mass $M = -10$ meV, which gives rise to helical edge states as illustrated in Figs. 1(a) and 1(b). An electric field $F \sim 10^{-3}$ mV/nm along \hat{x} is introduced by the time-dependent vector potential $eA(t) = -eFt\hat{x}$ via minimal coupling, $\mathbf{k} \rightarrow \mathbf{k} - eA(t)/\hbar$. This gauge preserves (k_x, k_y) as good quantum numbers in bulk, but it makes $H \rightarrow H_t$ time-dependent.

For finite ribbons, the confinement is introduced via a y -dependent mass potential [29,30] $M \rightarrow M(y)$ given by

$$M(y) = M_i + (M_o - M_i) \left[1 \pm \frac{1}{2} \tanh \left(\frac{y \pm W/2}{\gamma} \right) \right], \quad (2)$$

where M_i is the mass gap of the system, M_o is the mass of the confining barriers, and γ specifies whether the potential profile is sharp ($\gamma \rightarrow 0$) or smooth. Unless otherwise specified, we consider the hard-wall limit, which corresponds to $\gamma \rightarrow 0$ and $M_o \rightarrow \infty$. Due to the confinement, k_y is now quantized.

III. LANDAU-ZENER TUNNELING

The original Landau-Zener formula [1–5], developed for a pair of linear bands anticrossing, can be directly applied to the pair of hybridized edge-state branches arising in the ribbon

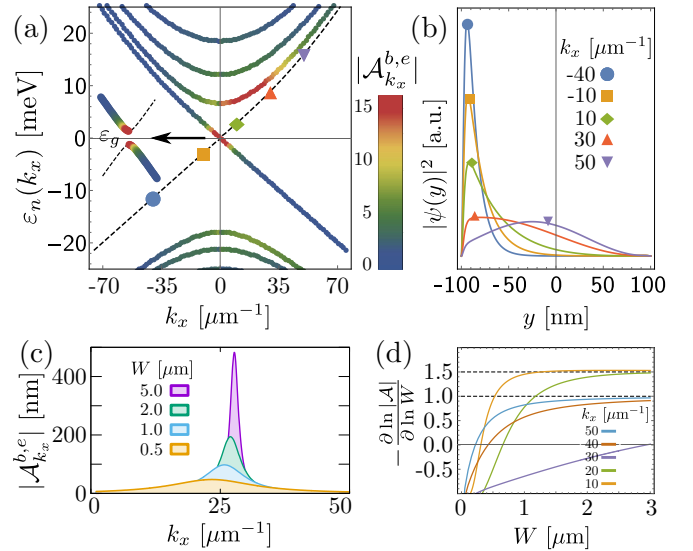


FIG. 2. (a) Band structure $\varepsilon_n(k_x)$ of a $W = 200$ nm ribbon. The color code in each band represents its Berry connection coupling $|\mathcal{A}_{k_x}^{b,e}|$ (in nm) to the selected edge branch (dashed). The inset at $k_x \approx 0$ shows the small hybridization gap $\varepsilon_g = 0.4$ meV. (b) Probability density of the edge state for different k_x 's, indicated by the symbols. As k_x increases, the state becomes extended (bulklike). (c) $|\mathcal{A}_{k_x}^{b,e}|$ between the first bulk quantized conduction band and the edge branch. As W increases, the peak becomes sharp at $k_x = k_c \approx 28\mu\text{m}^{-1}$. (d) Logarithmic derivative of $\ln |\mathcal{A}_{k_x}^{b,e}|$ with respect to W . For large $W \gg \ell$ ($\ell \approx |A/M| = 37.5$ nm), $|\mathcal{A}_{k_x}^{b,e}| \propto W^{-3/2}$ for $k_x < k_c$ and $|\mathcal{A}_{k_x}^{b,e}| \propto W^{-1}$ for $k_x > k_c$.

geometry [see the gap ε_g in the inset of Fig. 2(a)]. Therefore the tunneling probability between edge states is given by

$$\gamma_{ee} \approx \exp \left[- \frac{2\pi\varepsilon_g^2}{\hbar v_f e F} \right], \quad (3)$$

where $v_f \approx A/\hbar$ is the Fermi velocity of the nearly linear-in- k_x edge branches. Next we analyze the LZT between edge and bulk states.

Consider the time-dependent Hamiltonian H_t in the presence of an electric field as discussed above. Since $[H_t, k_x(t)] = 0$, we can write the solution as $\Psi(x, y, t) = e^{ik_x(t)x} \psi_{k_x(t)}(y, t)$. The unknown term $\psi_{k_x(t)}(y, t)$ can be expanded into Houston functions [31] $\varphi_{k_x(t),n}(y)$, which are solutions of an instantaneous Schrödinger equation $H_t \varphi_{k_x(t),n}(y) = \varepsilon_n[k_x(t)] \varphi_{k_x(t),n}(y)$, with n labeling both the quantized bulk bands ($n = b$) and the helical edge states ($n = e$) shown in Fig. 2. Since t is taken as a simple parameter in this auxiliary equation, $\varepsilon_n(k_x)$ is the band structure of the BHZ ribbon in the absence of an electric field. Ultimately, the Houston functions provide a complete time-dependent basis set, such that the full expansion reads

$$\psi_{k_x(t)}(y, t) = \sum_n \alpha_n(t) \varphi_{k_x(t),n}(y), \quad (4)$$

in which $\alpha_n(t)$ are time-dependent coefficients. Applying this expansion to the time-dependent Schrödinger equation,

we obtain

$$\left[i\hbar \frac{\partial}{\partial t} - \varepsilon_n(k_x(t)) \right] \alpha_n(t) = -eF \sum_{n'} \mathcal{A}_{k_x(t)}^{n,n'} \alpha_{n'}(t), \quad (5)$$

where $\mathcal{A}_{k_x(t)}^{n,n'} = i \langle k_x, n | \frac{\partial}{\partial k_x} | k_x, n' \rangle |_{k_x \rightarrow k_x(t)}$ are the (n, n') elements of the Berry connection matrix, and $|k_x, n\rangle$ is the Dirac ket for the Houston function $\varphi_{k_x, n}(y)$. For $n \neq n'$ ($\varepsilon_n \neq \varepsilon_{n'}$), $\mathcal{A}_{k_x(t)}^{n,n'}$ can be written as

$$\mathcal{A}_{k_x(t)}^{n,n'} = \frac{i}{\varepsilon_{n'} - \varepsilon_n} \left\langle k_x, n \left| \frac{\partial H}{\partial k_x} \right| k_x, n' \right\rangle \Big|_{k_x \rightarrow k_x(t)}, \quad (6)$$

which is most relevant near band anticrossings as $\varepsilon_n(k_x(t)) \approx \varepsilon_{n'}(k_x(t))$. These nondiagonal terms connect different eigenstates (n, n') via the electric field eF , i.e., it leads to the Landau-Zener tunneling. If restricted to a single band n , the usual diagonal Berry connection $\mathcal{A}_{k_x(t)}^{n,n}$ and Eq. (5) describe the adiabatic time evolution, while the complete expression for many bands fully describes the quantum unitary evolution.

In general, the LZT probabilities are obtained by solving Eq. (5) using the steepest descent approximation [31] around the extremum of the energy difference $\Delta \varepsilon_{nn'} = \varepsilon_n(k_x(t)) - \varepsilon_{n'}(k_x(t))$, assuming that $\mathcal{A}_{k_x(t)}^{n,n'}$ varies slowly so it can be approximated by its value at $\Delta \varepsilon_{nn'} = 0$. Here we cannot apply this method since bulk- and edge-state dispersions approach each other asymptotically as k_x increases. Instead, we focus on the properties of the couplings $\mathcal{A}_{k_x(t)}^{n,n'}$ shown in Figs. 2(a), 2(c), and 2(d).

Interestingly, for $W \gg \ell$, in which ℓ is the localization length of the edge states, the LZT between edge and bulk bands vanishes. This can be seen already from the normalization of these states. For an extended bulk state, the normalization goes as $\propto 1/\sqrt{W}$. On the other hand, the edge states $(|k_x, e\rangle \propto e^{-\tilde{y}/\ell}$ for an edge at $\tilde{y} = y - W/2 \approx 0)$ are localized within a length scale $\ell \equiv \ell(k_x)$ from the edges [see Figs. 1(a) and 2(b)]; at $k_x = 0$, $\ell(0) \approx |A/M|$ [29]. In this case, the edge-state normalization does not depend on the ribbon width. Additionally, the overlap between bulk- and edge-state wave functions is only finite near the edge, where the bulk state is qualitatively $|k_x, b\rangle \propto \frac{1}{\sqrt{W}} \sin(\pi \tilde{y}/W) \approx \pi \tilde{y}/W^{3/2}$, therefore the coupling $\mathcal{A}_{k_x(t)}^{b,e} \propto W^{-3/2}$; this is valid for small k_x . As k_x increases, the edge states become extended; see Figs. 2(a) and 2(b). Indeed for a semi-infinite system [32,33], k_y switches from purely imaginary (evanescent wave with $\ell = \text{Im}\{k_y\}^{-1}$) to purely real (bulklike, oscillatory wave) at the $k_x = k_c$ point, where the linear edge branch enters the bulk band. Consequently, for $k_x > k_c$ the normalization of the edge branch becomes bulklike, i.e., $\propto 1/\sqrt{W}$, and the coupling scales as $\mathcal{A}_{k_x(t)}^{b,e} \propto W^{-1}$. Both scalings yield a vanishing $\mathcal{A}_{k_x(t)}^{b,e}$ for large W .

The numerical evaluation shown in Fig. 2 confirms the asymptotic scalings of $\mathcal{A}_{k_x(t)}^{b,e}$. In Fig. 2(a) we calculate the coupling from a reference edge branch (dashed line) to all other edge and confined ribbon bands. The coupling intensity is indicated by the color code. The coupling $|\mathcal{A}_{k_x(t)}^{e,e'}|$ between the edge states is approximately a Lorentzian peak with broadening $\sim |2M/A|$ and intensity $\sim |A/\varepsilon_g|$ at $k_x = 0$. For large $W \rightarrow \infty$, this coupling diverges as the gap closes,

$\varepsilon_g = \varepsilon_n - \varepsilon_{n'} \rightarrow 0$. Similarly, in Figs. 2(a) and 2(c), the coupling between the dashed edge branch and the first bulk band shows a sharp peak for $W \rightarrow \infty$ at $k_x = k_c$, which matches the point where the edge branch transitions from localized to extended [Fig. 2(b)].

In Fig. 2(d) we show the logarithmic derivative of the coupling, which for $\mathcal{A}_{k_x(t)}^{b,e} \propto W^{-p}$ yields $-\frac{\partial \ln \mathcal{A}}{\partial \ln W} = p$. For $k_x < k_c$, all lines approach $p = 3/2$ asymptotically, while for $k_x > k_c$ they approach $p = 1$. These scalings show that already for $W \approx 1 \mu\text{m}$ the coupling between bulk and edge states is negligible. Effectively, there is no LZT between edge and bulk states for large samples.

IV. ZITTERBEWEGUNG

The zitterbewegung is the oscillatory motion of the mean value of the coordinates $\langle x \rangle(t)$, $\langle y \rangle(t)$, which is usually calculated in the broad wave-packet (plane-wave) limit, $\psi(t) \propto \exp[i\mathbf{k}(t) \cdot \mathbf{r}]$. To gain further insight about the ballistic dynamics of wave packets in TIs, we calculate these trajectories using the Ehrenfest theorem [34]. Omitting the time argument for brevity, i.e., $\langle O \rangle \equiv \langle O \rangle(t) = \langle \psi(t) | O | \psi(t) \rangle$, the coupled set of equations of motion reads

$$\frac{d\langle x \rangle}{dt} = -\frac{2}{\hbar} (D + B\langle \sigma_z \rangle) k_x(t) + \frac{As}{\hbar} \langle \sigma_x \rangle, \quad (7)$$

$$\frac{d\langle y \rangle}{dt} = -\frac{2}{\hbar} (D + B\langle \sigma_z \rangle) k_y^0 + \frac{A}{\hbar} \langle \sigma_y \rangle, \quad (8)$$

$$\frac{d\langle \boldsymbol{\sigma} \rangle}{dt} = \frac{2}{\hbar} \boldsymbol{\Omega} \times \langle \boldsymbol{\sigma} \rangle, \quad (9)$$

where the pseudospin $\langle \boldsymbol{\sigma} \rangle(t)$ precession is given by the vector $\boldsymbol{\Omega}(t) = \{sAk_x(t), Ak_y^0, M - B|\mathbf{k}(t)|^2\}$, with $k_x(t) = k_x^0 + eFt/\hbar$, and (k_x^0, k_y^0) are the initial momentum. The initial pseudospin $\langle \boldsymbol{\sigma} \rangle(0) = \boldsymbol{\sigma}^0$ is arbitrary. For simplicity, we take $x(0) = y(0) = 0$. The equations above show that the dynamics of $\langle x \rangle(t)$ and $\langle y \rangle(t)$ have contributions from $\langle \sigma_x \rangle(t)$ and $\langle \sigma_y \rangle(t)$. These oscillate due to the pseudospin precession given by Eq. (9), which gives rise to the zitterbewegung. Note that even for $k_y^0 = 0$, a finite transverse dynamics is set by the $\langle \sigma_y \rangle(t)$ contribution to $\langle y \rangle(t)$.

In the presence of the electric field, all possible initial conditions lead to a finite ballistic side-jump. This can be seen from the equations of motion noticing that, as time flows, $k_x(t)$ grows and the pseudospin precession is dominated by the z component of $\boldsymbol{\Omega}(t) \approx \{0, 0, -Bk_x^2(t)\}$. Therefore, $\langle \sigma_z \rangle(t)$ asymptotically approaches a constant σ_z^∞ , while $\langle \sigma_x \rangle(t)$ and $\langle \sigma_y \rangle(t)$ precess around a zero average with increasing frequency $2\Omega_z(t)/\hbar$. The final value for σ_z^∞ strongly depends on the initial conditions, ultimately affecting the asymptotic velocities in Eqs. (7) and (8). More importantly, the contributions from the last terms of these equations vanish on a time average, thus ceasing the zitterbewegung and the transverse dynamics, resulting in a finite side-jump $y(\infty)$.

To express $y(\infty)$, let us analyze Eqs. (7)–(9) in the limits of small and large M . First, recall that the Landau-Zener tunneling is characterized by the Berry connection. In bulk, this coupling intensity is $|eFA| \propto |eFA/M|$ at $\mathbf{k} = \mathbf{0}$, which becomes relevant if $|eFA| \gg |2M|$ (band gap). For large and

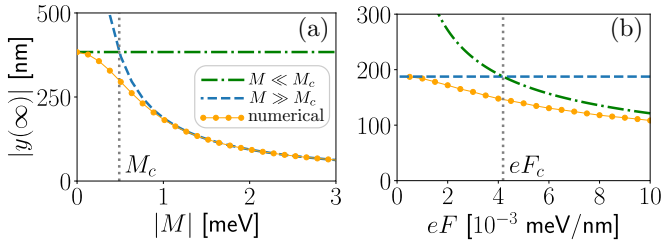


FIG. 3. The asymptotic limit $|y(\infty)|$ of the finite ballistic side-jump as a function of (a) M and (b) eF . For large $M \gg M_c$ (or $eF \ll eF_c$), the LZT is suppressed and the side-jump is independent of eF . In panel (a) we use $eF = 10^{-3}$ meV/nm, and in (b) $|M| = 1$ meV. In both cases, $\mathbf{k}^0 = \mathbf{0}$, $s = \uparrow$, and $\sigma_z^0 = \uparrow$. The dashed lines are the limiting cases from Eq. (10), while the vertical dotted line marks the critical mass M_c or electric field eF_c . The circles (orange) are the numerical data, which transit between both limiting cases.

small M , we find

$$|y(\infty)| \approx \begin{cases} \sqrt{\frac{A\pi}{8eF}} & \text{for } |M| \ll M_c, \\ \frac{A}{2|M|} & \text{for } |M| \gg M_c. \end{cases} \quad (10)$$

The transition point is defined by a critical mass $M_c \equiv \sqrt{2AeF/\pi}$, or critical field $eF_c \equiv \pi M^2/2A$. The solution for $M \ll M_c$ can be obtained analytically from Eqs. (7)–(9), while for $M \gg M_c$ the expression above was extracted from fitting the numerical data. These expressions are compared to the numerical data in Fig. 3 with great accuracy.

The Ehrenfest dynamics for $M = -10$ meV, different initial spin $s = (\uparrow, \downarrow)$, and pseudospin $\sigma_z^0 = (\uparrow, \downarrow)$ are shown in Fig. 1(c) for $0 < t < 5$ ps. The initial momentum is $(k_x^0, k_y^0) = (10^{-3}, 0)\text{nm}^{-1}$ in all cases. The trajectories show the oscillatory behavior (zitterbewegung) due to the pseudospin precession. Note that since $k_y^0 = 0$, all the dynamics along the transverse direction (y) are induced by $\langle \sigma_y \rangle(t)$ in Eq. (8). As discussed above, for large t , the trajectories bend inward as the transverse motion saturates. The zitterbewegung vanishes for $t \gtrsim 50$ ps with a finite side-jump of $|y(\infty)| \approx A/2|M| = 18.75$ nm.

The initial pseudospin σ^0 also affects significantly the dynamics. In Fig. 4(a) we consider σ^0 as the eigenstates of σ_x , which we label as $\sigma_x^0 = \{\Rightarrow, \Leftarrow\}$. Since at $\mathbf{k} \approx \mathbf{0}$, $\boldsymbol{\Omega}(t) \parallel \hat{z}$, the precession is approximately a circular motion of $\langle \sigma_x \rangle(t)$ and $\langle \sigma_y \rangle(t)$ on the $\langle \sigma_z \rangle = 0$ plane of the pseudospin Bloch sphere. This yields the nearly circular motion seen in Fig. 4(a) for $M = -1$ meV, which is distorted by the electric field $F = 10^{-3}$ mV/nm. As time flows, the circular motion ceases and converges toward a side-jump of $\sim \pm 200$ nm. For $M = -10$ meV, the dynamics is qualitatively equivalent to Fig. 4(a), but with a much faster precession that becomes difficult to visualize. Figures 1(c) and 4(a) were obtained for $M < 0$. However, nearly identical results are obtained in the trivial regime ($M > 0$) simply by mirroring $x \rightarrow -x$.

In Fig. 4(b) we use a crude approximation to show that the Ehrenfest Eqs. (7)–(9) would lead to skipping orbits at the edges for both trivial and nontrivial topological regimes. This would yield the absurd conclusion that one should expect edge

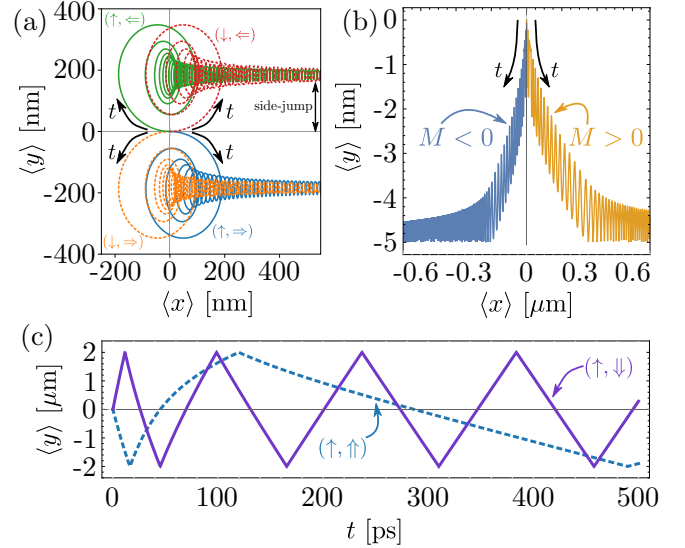


FIG. 4. (a) Bulk zitterbewegung trajectories for $M = -1$ meV, $\mathbf{k}^0 = \mathbf{0}$, and different initial spins $s = \{\uparrow, \downarrow\}$ and pseudospins $\sigma_x^0 = \{\Rightarrow, \Leftarrow\}$, as indicated. The reduced M leads to a larger side-jump $\sim \pm 200$ nm. (b) Incorrect skipping orbits at the edge ($y = -5$ nm) appear for both trivial ($M > 0$) and nontrivial ($M < 0$) topological regimes if the Ehrenfest equations (7)–(9) are used beyond their limit of validity. Here $(k_x^0, k_y^0) = (10^{-3}, 0)\text{nm}^{-1}$, initial $(s, \sigma_z^0) = (\uparrow, \uparrow)$, and $M = \pm 10$ meV. (c) Qualitative zitterbewegung $\langle y \rangle$ vs t on a large $W = 4\mu\text{m}$ ribbon for different initial conditions $s = \uparrow$ and $\sigma_z^0 = \{\uparrow, \downarrow\}$. In all cases, $(k_x^0, k_y^0) = (10^{-3}, 10^{-2})\text{nm}^{-1}$, $M = -10$ meV. At the edges $y = \pm W/2$, the trajectory bounces with specular reflection as $k_y \rightarrow -k_y$ and $\langle \sigma_y \rangle \rightarrow -\langle \sigma_y \rangle$ in Eq. (8).

states in both trivial and nontrivial topological regimes. These results are misleading. Here we correctly consider specular reflections at the edges by flipping the velocity sign when there is a collision, i.e., $k_y^0 \rightarrow -k_y^0$ and $\langle \sigma_y \rangle \rightarrow -\langle \sigma_y \rangle$ in Eq. (8), which is consistent with the pseudospin texture of the bulk band structure. However, the Ehrenfest equations only return a closed set of equations if one considers the plane-wave limit, such that \mathbf{k} is a good quantum number. In the opposite limit, for narrow wave packets, significant deviations are expected [16]. This means that to use the Ehrenfest equations above, one must assume that they describe the center of motion of a broad packet. Moreover, for reasonable values of M ($= \pm 10$ meV), the finite side-jump is only $|y(\infty)| \approx 20$ nm, which is much smaller than the required packet broadening ($\sim 1\mu\text{m}$). Therefore, the trajectories in Fig. 4(b) are not compatible with the approximations that validate Eqs. (7)–(9), hence the skipping orbits shown in Fig. 4(b) are not accurate.

Nonetheless, the Ehrenfest Eqs. (7)–(9) can be applied for a finite ribbon of width W if one considers the initial packet to be a broad enough Gaussian packet. This requires W to be even larger, so that the ribbon can accommodate the initial packet. For the typical set of parameters, this requires an initial Gaussian broadening $\Gamma > 1\mu\text{m}$, which also guarantees that the packet broadening is nearly constant in time. The resulting motion is to be seen as qualitative, since it does not consider the broadening explicitly.

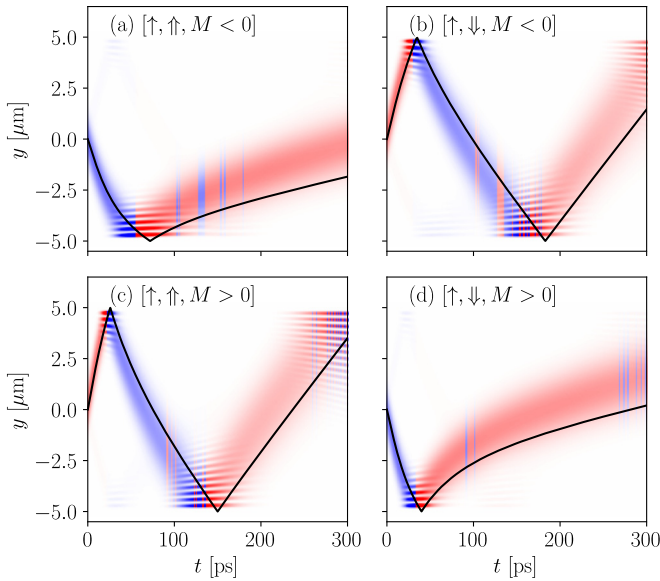


FIG. 5. Time evolution of the density $|\psi(y, t)|^2$ and its corresponding Ehrenfest trajectory $\langle y \rangle(t)$ (black line) for a $W = 10 \mu\text{m}$ ribbon [other parameters are equivalent to those in Fig. 4(c)]. The spin is $s = \uparrow$, and the initial pseudospin $\sigma_z = \{\uparrow, \downarrow\}$ is indicated in each panel. The top (bottom) panel shows the dynamics in the nontrivial (trivial) regime, $M = -10$ meV ($M = 10$ meV). In all cases, the packets bounce at the edges $y = \pm W/2$. The blue and red colors indicate the sign of $\langle \sigma_y \rangle$ (time-averaged over a few periods around each t). A small numerical noise is seen in the color code due to the fast oscillation of $\langle \sigma_y \rangle$.

Let us consider $W = 4 \mu\text{m}$. Since the side-jump is in the nanometer range, an initial packet with $k_y^0 = 0$ would never reach the edges at $y = \pm W/2$. Hence a finite $k_y^0 \neq 0$ is necessary to lead to a collision of the packet with the edge. The resulting dynamics are shown in Fig. 4(c). At the edges $y = \pm W/2$, we consider the specular reflection described above. For any set of realistic parameters, we see the trajectories bouncing at the edges with no signature of skipping orbits. The differences between the trajectories in Fig. 4(c) arise from the broken electron-hole symmetry of H , while for $D = 0$ they become identical. These results agree with the full quantum dynamics of a Gaussian wave packet shown in Fig. 5, which we discuss next.

V. WAVE-PACKET DYNAMICS

The Houston states provide a clear interpretation of the couplings $A_{k_x(t)}^{n, n'}$ that lead to the LZT, while the zitterbewegung, calculated via the Ehrenfest equations, gives us insight about the dynamics of a wave packet. To complement these results, we now solve the time-dependent Schrödinger equation numerically to observe the dynamics of a wave packet as it collides with the edge of the system. We are interested in wide ribbons in the micrometer range, so here we consider the memory-efficient split-operator method [35], which is based on the Suzuki-Trotter expansion [36,37]. The approximate time-evolution operator is given by

$$U(t + \tau, t) \approx e^{-iV_y \frac{\tau}{2\hbar}} e^{-iT_k(t) \frac{\tau}{\hbar}} e^{-iV_y \frac{\tau}{2\hbar}} + O(\tau^3), \quad (11)$$

where $V_y = M(y)\sigma_z$ is the single y -dependent term of H_t [see Eq. (2)], while $T_k(t)$ contains all k -dependent contributions from Eq. (1). For the initial state, Eq. (4) now becomes a Gaussian wave packet with broadening Γ and initial momentum (k_x^0, k_y^0) , which reads

$$\psi(y, 0) = e^{ik_y^0 y} \frac{\exp(-\frac{y^2}{4\Gamma^2})}{(2\pi\Gamma^2)^{1/4}} \xi_\sigma, \quad (12)$$

where ξ_σ is the vector representation of the initial spin σ^0 , e.g., $\xi_\uparrow = \begin{pmatrix} 1 \\ 0 \end{pmatrix}$, $\xi_\downarrow = \begin{pmatrix} 0 \\ 1 \end{pmatrix}$. As time flows, the packet broadens approximately as $\Gamma_t = \sqrt{\Gamma^2 + [2(D \pm B)t/\Gamma\hbar]^2}$. As usual, an initially narrow packet broadens quickly, while for initial $\Gamma \gg [2(D \pm B)t/\Gamma\hbar]^{1/2}$ it remains $\Gamma_t \approx \Gamma$ within $0 < t < t_f \sim 500$ ps. For our typical set of parameters, this condition requires $\Gamma \geq 1 \mu\text{m}$. Hereafter, we consider $\Gamma = 1 \mu\text{m}$.

For $k_y^0 = 0$, the transverse motion is limited to the ~ 20 nm side-jump, which is much smaller than $\Gamma \sim 1 \mu\text{m}$, making it difficult to visualize the overall motion. Nonetheless, in this case the center of motion of the wave packet matches the zitterbewegung trajectories, Figs. 1(c) and 4(a), obtained with the Ehrenfest equations. Due to the short side-jump, this bulk dynamics does not reach the edges.

For $k_y^0 \neq 0$ the results are shown in Fig. 5. One immediately sees that the packet bounces off the borders unaffected by the presence of the edge states. Essentially there is no qualitative difference between the dynamics in the trivial ($M > 0$) and nontrivial ($M < 0$) topological regimes. Moreover, in all cases, the packet evolution agrees well with the Ehrenfest dynamics for equivalent initial conditions (black lines in Fig. 5). The good agreement with the Ehrenfest trajectories emphasizes that edge states play no role in the dynamics of a packet initially set in bulk. The color code of the packet densities in Fig. 5 indicates the sign of $\langle \sigma_y \rangle$ obtained from the Schrödinger time evolution. As the packet bounces off the borders, $\langle \sigma_y \rangle \rightarrow -\langle \sigma_y \rangle$ and $k_y \rightarrow -k_y$, thus justifying the specular reflection introduced in the Ehrenfest dynamics above.

VI. CONCLUSIONS

We have shown that topological edge states effectively do not couple to bulk states via LZT. This conclusion arises exactly from the Houston function approach for the time evolution that relates the LZT to the Berry connection matrix element $A_{k_x}^{n, n'} \propto W^{-p}$, with $p = 3/2$ (1) for small (large) k_x . Numerical evaluation of $A_{k_x}^{n, n'}$ confirms these scalings. Additionally, the zitterbewegung and numerical wave-packet time evolution were developed to further investigate the dynamics. These show packets bouncing off the edges in both trivial and nontrivial topological regimes. More interestingly, the zitterbewegung dynamics show that all possible initial conditions lead to a finite ballistic side-jump. Overall, these results contrast those from Ref. [19], where the zitterbewegung was introduced as a semiclassical picture for the topological helical edge states that yield the edge magnetization of the QSHE. Instead, for narrow ribbons the zitterbewegung can be associated with a ballistic SHE [27].

In a diffusive regime, we expect this dynamics to be consistent with the Rashba-Edelstein effect [16,28], which

might lead to spin accumulation at the edges (i.e., SHE) in both trivial and nontrivial topological regimes. This yields an interesting scenario, where there could be an interplay between the QSHE in SHE, depending on the chemical potential and how the electrons are injected into the sample. It is important to emphasize that here we have considered only the edge-bulk coupling via LZT, while other couplings could play a significant role [38]. The full diffusive

dynamics in a ribbon geometry with bulk and edge states considered on an equal footing remains both unexplored and challenging.

ACKNOWLEDGMENTS

The authors acknowledge support from CAPES, CPNq, FAPEMIG, FAPESP, and NAP Q-NANO from PRP/USP.

-
- [1] L. D. Landau, On the theory of energy transmission in collisions I, *Phys. Z. Sowjet.* **1**, 88 (1932).
- [2] L. D. Landau, On the theory of transfer of energy at collisions II, *Phys. Z. Sowjet.* **2**, 46 (1932).
- [3] C. Zener, Non-adiabatic crossing of energy levels, *P. R. Soc. London, Ser. A* **137**, 696 (1932).
- [4] E. C. G. Stueckelberg, Theorie der unelastischen Stöße zwischen atomen, *Helv. Phys. Acta* **5**, 369 (1932).
- [5] E. Majorana, Atomi orientati in campo magnetico variabile, *Nuovo Cimento* **9**, 43 (1932).
- [6] S. M. Frolov, S. Luescher, W. Yu, Y. Ren, J. A. Folk, and W. Wegscheider, Ballistic spin resonance, *Nature (London)* **458**, 868 (2009).
- [7] M. O. Hachiyā, G. Usaj, and J. C. Egues, Ballistic spin resonance in multisubband quantum wires, *Phys. Rev. B* **89**, 125310 (2014).
- [8] J. Schliemann, J. C. Egues, and D. Loss, Nonballistic Spin-Field-Effect Transistor, *Phys. Rev. Lett.* **90**, 146801 (2003).
- [9] B. A. Bernevig, J. Orenstein, and S.-C. Zhang, Exact $su(2)$ Symmetry and Persistent Spin Helix in a Spin-Orbit Coupled System, *Phys. Rev. Lett.* **97**, 236601 (2006).
- [10] J. D. Koralek, C. P. Weber, J. Orenstein, B. A. Bernevig, S.-C. Zhang, S. Mack, and D. D. Awschalom, Emergence of the persistent spin helix in semiconductor quantum wells, *Nature (London)* **458**, 610 (2009).
- [11] M. P. Walser, C. Reichl, W. Wegscheider, and G. Salis, Direct mapping of the formation of a persistent spin helix, *Nat. Phys.* **8**, 757 (2012).
- [12] M. Kammermeier, P. Wenk, and J. Schliemann, Control of Spin Helix Symmetry in Semiconductor Quantum Wells by Crystal Orientation, *Phys. Rev. Lett.* **117**, 236801 (2016).
- [13] J. Schliemann, Colloquium: Persistent spin textures in semiconductor nanostructures, *Rev. Mod. Phys.* **89**, 011001 (2017).
- [14] J. Schliemann, D. Loss, and R. M. Westervelt, Zitterbewegung of Electronic Wave Packets in III-V Zinc-Blende Semiconductor Quantum Wells, *Phys. Rev. Lett.* **94**, 206801 (2005).
- [15] J. Schliemann, D. Loss, and R. M. Westervelt, Zitterbewegung of electrons and holes in III-V semiconductor quantum wells, *Phys. Rev. B* **73**, 085323 (2006).
- [16] J. Schliemann, Ballistic side-jump motion of electrons and holes in semiconductor quantum wells, *Phys. Rev. B* **75**, 045304 (2007).
- [17] E. Bernardes, J. Schliemann, M. Lee, J. C. Egues, and D. Loss, Spin-Orbit Interaction in Symmetric Wells with Two Subbands, *Phys. Rev. Lett.* **99**, 076603 (2007).
- [18] C. S. Ho, M. B. A. Jalil, and S. G. Tan, Persistent Zitterbewegung of electron wave packet in time-dependent Rashba system, *Europhys. Lett.* **108**, 27012 (2014).
- [19] L.-K. Shi, S.-C. Zhang, and K. Chang, Anomalous electron trajectory in topological insulators, *Phys. Rev. B* **87**, 161115(R) (2013).
- [20] M. Kolodrubetz, B. M. Fregoso, and J. E. Moore, Nonadiabatic bulk-surface oscillations in driven topological insulators, *Phys. Rev. B* **94**, 195124 (2016).
- [21] A. Yar, M. Naeem, S. U. Khan, and K. Sabeeh, Hybridization effects on wave packet dynamics in topological insulator thin films, *J. Phys. Condens. Matter* **29**, 465002 (2017).
- [22] B. A. Bernevig, T. L. Hughes, and S.-C. Zhang, Quantum spin Hall effect and topological phase transition in HgTe quantum wells, *Science* **314**, 1757 (2006).
- [23] M. König, S. Wiedmann, C. Brüne, A. Roth, H. Buhmann, L. W. Molenkamp, X.-L. Qi, and S.-C. Zhang, Quantum spin Hall insulator state in HgTe quantum wells, *Science* **318**, 766 (2007).
- [24] M. Z. Hasan and C. L. Kane, Colloquium: Topological insulators, *Rev. Mod. Phys.* **82**, 3045 (2010).
- [25] X.-L. Qi and S.-C. Zhang, Topological insulators and superconductors, *Rev. Mod. Phys.* **83**, 1057 (2011).
- [26] S. I. Erlingsson and J. C. Egues, All-electron topological insulator in InAs double wells, *Phys. Rev. B* **91**, 035312 (2015).
- [27] P. Brusheim and H. Q. Xu, Spin Hall effect and zitterbewegung in an electron waveguide, *Phys. Rev. B* **74**, 205307 (2006).
- [28] G. Vignale and I. V. Tokatly, Theory of the nonlinear Rashba-Edelstein effect: The clean electron gas limit, *Phys. Rev. B* **93**, 035310 (2016).
- [29] P. Michetti, P. H. Penteado, J. C. Egues, and P. Recher, Helical edge states in multiple topological mass domains, *Semicond. Sci. Technol.* **27**, 124007 (2012).
- [30] G. J. Ferreira and D. Loss, Magnetically Defined Qubits on 3D Topological Insulators, *Phys. Rev. Lett.* **111**, 106802 (2013).
- [31] M. P. Marder, *Condensed Matter Physics* (John Wiley & Sons, Hoboken, NJ, 2010).
- [32] B. A. Volkov and O. A. Pankratov, Two-dimensional massless electrons in an inverted contact, *JETP Lett.* **42**, 178 (1985).
- [33] O. A. Pankratov, S. V. Pakhomov, and B. A. Volkov, Supersymmetry in heterojunctions—Band-inverting contact on the basis of $Pb_{1-x}Sn_xTe$ and $Hg_{1-x}Cd_xTe$, *Solid State Commun.* **61**, 93 (1987).
- [34] O. V. Prezhdo and Y. V. Pereverzev, Quantized Hamilton dynamics, *J. Chem. Phys.* **113**, 6557 (2000).
- [35] V_y is diagonal in real (y) space, while $T_k(t)$ is diagonal in reciprocal (k_y) space. To alternate between y and k_y spaces, we use FFT algorithms and apply each term of the time-evolution operator either in y or k_y space, hence minimizing the memory use. Additionally, since $T(t)$ is time-dependent, we consider a sufficiently short time-step τ to assure numerical convergence.
- [36] H. F. Trotter, On the product of semi-groups of operators, *Proc. Am. Math. Soc.* **10**, 545 (1959).

- [37] M. Suzuki, Generalized Trotter's formula and systematic approximants of exponential operators and inner derivations with applications to many-body problems, *Commun. Math. Phys.* **51**, 183 (1976).
- [38] C.-H. Hsu, P. Stano, J. Klinovaja, and D. Loss, Nuclear-spin-induced localization of edge states in two-dimensional topological insulators, *Phys. Rev. B* **96**, 081405(R) (2017).